Hemispherical reflectance and albedo estimates from the accumulation of across-track sun-synchronous satellite data

Marie Weiss,[1] Frédéric Baret ,[1] Marc Leroy ,[2] Agnès Bégué,[3] Olivier Hautecoeur,[2] and Richard Santer,[4]

Abstract. The estimation of the hemispherical reflectance and the instantaneous albedo of canopies from top of canopy satellite reflectance data was investigated. The study was designed to approximate the specifications of generic sensors aboard satellites like NOAA, VEGETATION, MERIS, MISR, MODIS, and PRISM. These sensors acquire reflectance data in two to six wave bands distributed along the visible, near-infrared, and middle infrared domains. Five great biomes (grassland, sparse vegetation, tropical forest, boreal forest, and bare soil) were approximated, simulating the corresponding top of canopy reflectances as observed from the satellites using well-known leaf, soil, and canopy radiative transfer models, including the effect of cloud cover that limits the actual data acquisition scheme. Albedo was accurately derived from the hemispherical reflectance observed in only a few wave bands. When using six wave bands, albedo was estimated within 1% relative accuracy. The MRPV bidirectional reflectance distribution function (BRDF) model was tested to derive the hemispherical reflectance from the top of canopy bidirectional data as sampled by the generic sensors during a 32 day orbit cycle. Results showed that this is the main source of error, with a relative accuracy around 6%. This showed the importance of the directional sampling scheme and possible improvements that may be made to the model and the way it is fitted to the observed data. The algorithm developed produced a relative accuracy less than 7% for the albedo estimation, when using the six wave bands and a ±45° across-track directional scanning capacity. The results were discussed with particular emphasis on the optimization of sensors and algorithms dedicated to albedo estimation and to the use of hemispherical reflectance as a potential normalized geophysical product for monitoring vegetation.

1. Introduction

Albedo is one of the most important variables required as a primary input for global circulation models used to forecast short-term weather and long-term climatic change [*Dickinson,* 1983]. It is also mandatory for local and regional estimates of energy and mass exchanges between the earth surface and the atmosphere, as described by soil- vegetation-atmosphere-transfer models [*Olioso et al.,* 1999]. Albedo is the amount of solar energy reflected by a surface. It provides information on the radiative balance and thus on temperature and water balance also. Instantaneous albedo is a dimensionless biophysical characteristic of the canopy. It is expressed as the ratio of the radiant energy scattered upward by a surface in all directions, compared to that received from all directions (direct and scattered by the atmosphere solar radiation), integrated over wavelengths of the solar spectrum [*Pinty and*

[1] Institut National de la Recherche Agronomique, Bioclimatologie, Avignon, France.
[2] Centre d'Etudes Spatiale de la BIOsphère, Toulouse, France
[3] Centre de Coopération Internationale en Recherche Agronomique pour le Développement, Montpellier, France
[4] Laboratoire d'Optique Atmosphérique, Université du littoral, Wimereux, France.

Verstraete, 1992]. Albedo depends on the irradiance conditions and thus varies constantly throughout the day [*Kimes et al.,* 1987]. Two types of albedo can be estimated: black sky albedo, corresponding only to the direct radiation coming from the Sun, and a white sky albedo corresponding roughly to the diffuse radiation assumed isotropic [*Strahler et al.,* 1996]. *Henderson-Sellers and Wilson* [1983] demonstrated from a sensitivity analysis that, for climate modeling, a relative accuracy of ±5% is required for albedo values for all types of cover.

Satellite data provide a very convenient way to monitor albedo values at local to regional scales. Over the next few years, several satellites, POLDER, MERIS, VEGETATION, SEAWIFS, MODIS, MISR, PRISM and MSG, will have pertinent spatial, temporal, directional, and spectral capacities for obtaining accurate albedo estimates. Dedicated algorithms for albedo estimation are thus required.

Single, bidirectional measurement of reflectance in a selection of wave bands is not usually representative of the actual instantaneous albedo of a surface since albedo is the integration of the bidirectional reflectance over the whole upward hemisphere (hemispherical reflectance or spectral albedo) and over the whole optical spectral domain (300-3000 nm). Obtaining this requires the observation of the same surface under all directions and all wave bands. This is not possible with usual satellite-borne systems. Thus a multiplicity of models describing the bidirectional reflectance distribution function (BRDF) have been developed to interpolate or extrapolate between the actual view and solar

directions sampled by the satellite to derive the full BRDF. Similarly, algorithms for extrapolating the spectral response in bands not sampled by the satellite have to be developed.

Several linear or semilinear models have been proposed in recent years to describe reflectance as a function of illumination and viewing conditions [Strahler et al., 1996]. They range from empirical ones [Shibayama and Wiegand, 1985; Shibayama et al., 1985; Walthall et al., 1985] to semiphysical models [Roujean et al., 1992; Wanner et al., 1995; Engelsen et al., 1996].

For a view zenith angle θ_v, a solar zenith angle θ_s, and a relative azimuth angle $(\varphi = \varphi_v - \varphi_s)$, the BRDF can be expressed as

$$\rho(\theta_s, \theta_v, \varphi) = \sum_{m=1}^{m=M} \beta_m . k_m(\theta_s, \theta_v, \varphi), \qquad (1)$$

where M is the number of kernels $k_m(\theta_s, \theta_v, \varphi)$ of the model, each being associated with a weight β_m. The kernels are particular functions of the Sun and view directions.

These BRDF models must be analytically or numerically inverted over satellite reflectance data corresponding to a restricted number of view directions. The inversion process consists of tuning parameters such as the simulated reflectance matching the reflectance values measured in the selection of satellite view directions. The adjusted parameters of the model are later used to estimate the whole BRDF, thus the hemispherical reflectance and finally the albedo. Model inversion is a complex process. To reduce ambiguities and local minimum, only a limited number of parameters should be adjusted. That is the reason why only semiempirical and empirical models are used in this context, since physically based models require too many input variables or parameters and are demanding computer time.

Several studies have been conducted to estimate the albedo of a range of surfaces from remote sensing data. Earlier studies assumed terrestrial surfaces to be lambertian. *Kimes and Sellers* [1985] estimated the errors induced by this assumption on a variety of canopies and concluded that significant error was introduced. Thus they recommended using off-nadir reflectances to improve the accuracy of hemispherical reflectance estimates. This was performed by *Pinty and Ramond* [1986] who developed a simple semiempirical model to estimate the spectral albedo of land and desert from the Nimbus7 Earth radiation budget experiment. In the same way, *Wanner et al.* [1997] developed an algorithm for albedo estimation combining registered, multidate and multiband reflectance data from the EOS MODIS and MISR instruments, using the AMBRALS (Algorithm for MODIS bidirectional reflectance anisotropy of the land surface) BRDF model. *Privette et al.* [1997] and *Lucht* [1998] have already compared the ability of such models to extrapolate the BRDF in solar directions different from that corresponding to the observation.

The objective of this study was to develop an algorithm for the estimation of hemispherical reflectances and albedo from the next generation of satellite sensors that accumulate reflectance data in short time periods and in a range of view directions, using a few, well-distributed wave bands. Currently, this is achieved through across-track directional sampling, either for the large swath sensors, or for sensors with across-track depointing capacities. However, other directional sampling schemes could be used, such as those of POLDER [Deschamps et al., 1994] and MISR [Diner et al., 1998]. In this study, we focused on Sun-synchronous sensors with a 32 day cycle and considered across-track sampling up to ±30°, ±45°, ±50° at the satellite level. Six wave bands roughly corresponding to Landsat thematic mapper bands: blue (445 nm), green (560 nm), red (665 nm), near infrared (855 nm), and middle infrared (1650 nm and 2200 nm) were considered. We focused on the ability of a BRDF model to extrapolate the BRDF in viewing directions, allowing the computation of the hemispherical reflectance. We then developed a method, based on linear regression, to derive estimates of albedo from the hemispherical reflectance values observed in a selection of the wave bands considered.

Almost no measurements presenting the spatial, temporal, directional, and spectral characteristics considered above are currently available over a large range of cover types. Thus we created a "synthetic database" that represented a large variation of vegetation characteristics. This data set was obtained by using radiative transfer models based on a physical description of the processes governing light propagation. No accounting was made for the noise due to atmosphere, instrument characteristics, or images coregistration, which could be important.

2. Database Description

Five types of biomes that largely represent the Earth's surface were simulated: grassland, sparse vegetation (savanna), tropical forest, boreal forest and bare soil (clay/calcareous brown dry soil with three different roughness, sand, crust, litter and peat).

2.1. Description of the Canopy Radiative Transfer Model

The top of canopy BRDF simulations were performed with Myneni's radiative transfer model [Myneni et al., 1992]. It is one of the most powerful models since it takes into account heterogeneous canopies, non-Lambertian properties of leaves, specular effect, and hot spot feature. It is based on a numerical solution of the 3D radiative transfer equation by the method of discrete ordinates [Myneni et al., 1991]. The canopy is divided into layers of cubic cells defined by a leaf area density and the optical properties of the leaves. A leaf inclination distribution and a hot spot parameter define each horizontal layer. There is, however, no explicit description of the clumping within a cell or among cells that are close together. The soil background is also considered. The BRDF is discretized into 8x6 directions and is interpolated afterwards into a 24x24 Gaussian quadrature. The four submodels used in Myneni's reflectance model are the following (1) Leaf optical model, PROSPECT [Jacquemoud and Baret, 1990]: This provides the spectral variation (400-2500 nm) of the leaf hemispherical reflectance and transmittance as a function of chlorophyll and water contents, and a parameter characterizing the mesophyll structure. (2) Leaf specular model, Nilson's specular model [Nilson and Kuusk, 1989] : This model assumes that the leaves are flat mirrors and the specular component of the canopy originates from their surface. The specular reflectance depends thus on leaf inclination distribution in the canopy and an attenuation coefficient used to simulate the effects of hairs or roughness of the leaf surface. This specular component is assumed to contribute only to the single scattering. (3) Soil reflectance

model, SOILSPECT [*Jacquemoud et al.*, 1992]: This model simulates the spectral and bidirectional reflectance of a soil. It is derived from Hapke's [*Hapke.*, 1981, 1984, 1986] model and requires six parameters: a single-scattering albedo depending on the wavelength, four parameters describing the phase function, and a roughness parameter that describes the hot spot feature. (4) Hot spot model, *Verstraete et al.* [1990]: The hot spot effect induces an increase of reflectance, as no shadow is visible in that direction. It depends on the structure of the canopy and particularly on the size of the gaps between leaves. This model requires the "average radius of the gap, *r*": (*2rLAD*) is the ratio between the mean horizontal distance between leaves and the mean vertical distance between layers of leaves.

Myneni's model requires one additional input variable, the fraction of direct radiation. It was computed using an atmosphere radiative transfer model 5S [*Tanré et al.*, 1990], considering an average value of atmosphere characteristics (23 km visibility for aerosol scattering) coupled to the canopy radiative transfer.

2.2. Canopies Simulated

The above described models have been used to simulate a range of canopies corresponding to the biomes that predominate over the Earth's surface. We chose a combination of five canopy types (grassland, sparse vegetation, tropical forest, boreal forest, and bare soil) with three latitudes (0°, 30°, 60°). Obviously, all the combinations were not possible. For each canopy type, two or three soils were simulated with, high, medium, and low vegetation development, for three dates (Julian days 80, 172, and 355) corresponding to the evolution of the canopy during the year and from place to place. Table 1 presents the 77 canopy simulations. The choice of the model input parameters was driven mainly by results of several experiments such as HAPEX-SAHEL [*Goutorbe et al.*, 1994] for sparse vegetation and BOREAS [*Sellers et al.*, 1994] for boreal forests.

2.3. Directional Sampling Used

The directional sampling of a satellite is mainly driven by its orbitography, the swath, and the depointing capabilities of the instrument. We chose the orbital characteristics of the future PRISM sensor [*Del Bello et al.*, 1995] which is very similar to several other satellites (MERIS, VEGETATION,

MSG, NOAA, MISR, and MODIS). PRISM will have a circular orbit at an altitude of 786 km, an inclination angle of 98°47, a 32 day repeat cycle, and an equatorial node crossing time of 10:00 LT. Orbitography simulations provided high-frequency observations performed by across-track viewing according to three possible scenarios: ± 30°, ± 45°, and ± 50° view zenith angle at satellite level. Considering the altitude of the satellite and the Earth's rotundity, the maximum view angles actually increase from 30° to 34.5°, from 45° to 53°, and from 50° to 60° at the canopy level. The directional sampling was performed during the whole orbital cycle, centered at the date of the simulation (Figure 1). For a given latitude we notice a rotation of the diagram from date to date as the Sun azimuth changes, while the view directions remain the same: for example, at 30° latitude, we observe about 30° rotation of the diagram from March to June. The number of data available increases with the range of view angles (Figure 2). It increases also with the latitude, since for latitudes higher than 30°, the same point can be observed twice a day from two consecutive orbits. That explains the discontinuity observed at latitude 60° in the directional sampling scheme.

Due to cloud cover, the potential directional sampling scheme previously defined must be restricted to a selection of view directions. To take this effect into account, we simulated five image acquisition scenarios: we randomly selected 20%, 50%, 80%, 100% and International Satellite Cloud Climatology Project (ISCCP) percentage (Table 2) of the directional data to simulate the cloud cover. ISCCP data [*Rossow et al.*, 1988] provides the average cloudiness value at a given latitude and longitude, date, and time.

A catalogue of the top of canopy BRDF and the associated hemispherical reflectance of 77 land covers was available. The BRDF in six wave bands was computed for 24 x 24 directions and interpolated into the view angles that correspond to PRISM directional sampling, taking into account five cloud occurrence scenarios. This resulted in 1155 satellite simulations corresponding to 77 biomes × 3 directional sampling scenarios × 5 cloud cover scenarios.

3. Estimation of the Hemispherical Reflectance and Instantaneous Albedo

The simulated BRDF catalogue as sampled by the satellite was then used to develop a method of estimating hemispherical reflectance and thus albedo from the top of

Table 1. Combination of Latitudes, Day of the Year, Soil Types, and Total Leaf Area Index Values (Grass+Trees) of the Canopies Used for the Simulations

Canopy	Composition	0° Latitude DOY 172	30° Latitude			60° Latitude	
			DOY 80	DOY 172	DOY 355	DOY 80	DOY 172
Grassland (clay)		-	-	1-2-4	-	2-4	5-4-8
Sparse vegetation	20% grass	-	0.2-0.5	0.1-0.2	-	-	-
	40% grass, 20% trees	-	1.4-1.8	1.2-1.4	-	-	-
(sand, crust, litter)	60% grass, 40% trees	-	2.2-2.7	2.0-2.1	-	-	-
	20% trees	-	-	-	1.05	-	-
	40% trees	-	-	-	1.83	-	-
Tropical forest (peat)		3.5-6.3	-	-	-	-	-
Boreal forest (moss)		-	-	-	-	-	3.37

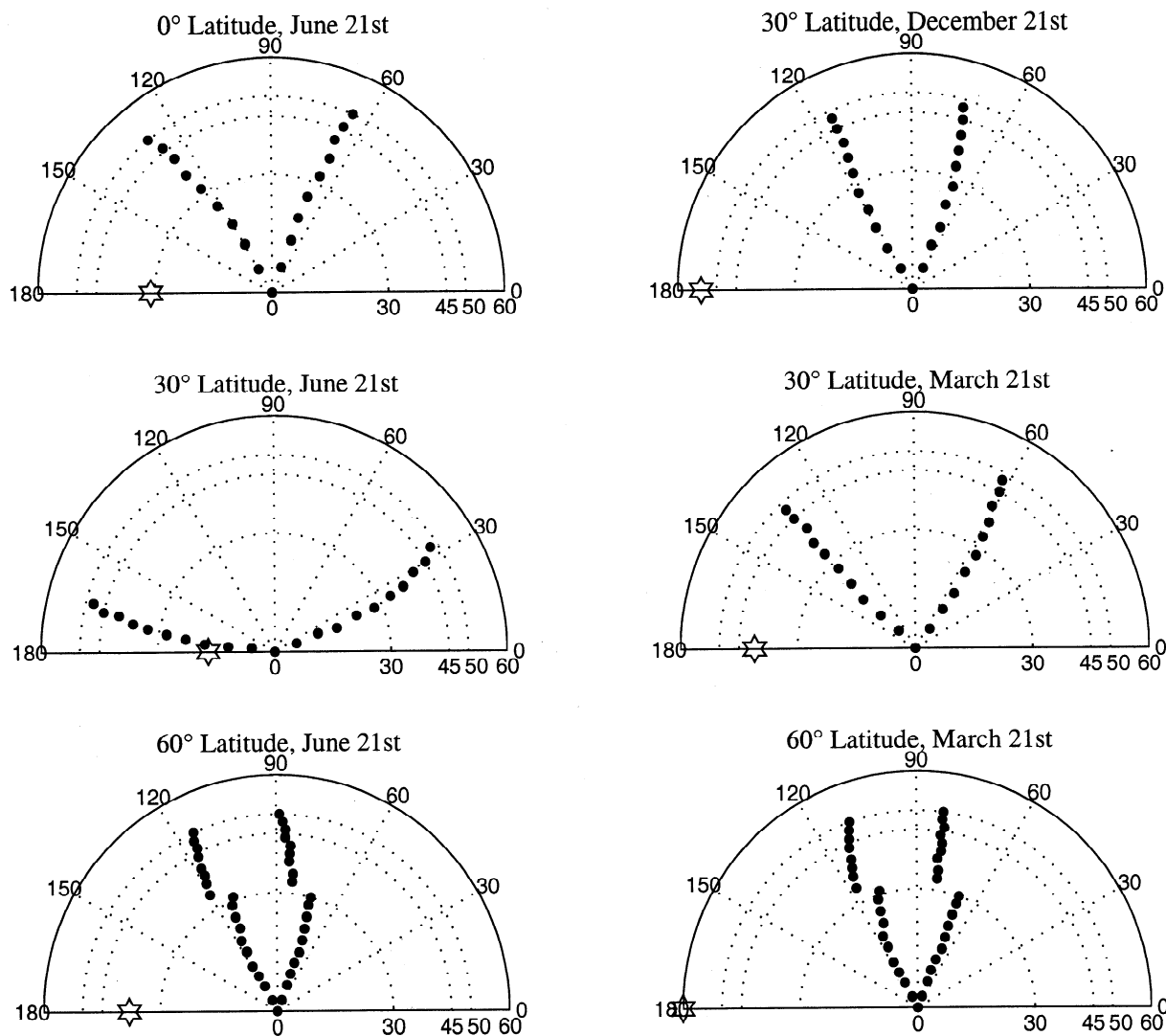Soil types are in parentheses. DOY, day of the year

Figure 1. Polar representation of the directional sampling used for the simulations for the three across-track scanning capacities at satellite level: ±30°, ±45°, and ±50°. The observations were accumulated during the PRISM orbital cycle (date of the simulation ± 16 days). The plane 0°-180° is the principle plane. The Sun position is represented by a star, and the satellite position is represented by solid circles.

canopy reflectance data. The instantaneous albedo of the canopy corresponds to the integration of the bidirectional reflectance over the view directions and over the whole 300-3000 nm spectral domain. These two issues are addressed separately, starting with the spectral integration issue.

3.1. Instantaneous Albedo Estimation From Hemispherical Reflectance in Few Wave Bands

The instantaneous albedo (a) corresponds to the spectrally integrated value between 300 and 3000 nm of the hemispherical reflectance $\rho_h(\lambda)$ weighted according to the incoming solar radiation at the top of canopy level $E(\lambda)$:

$$a = \frac{1}{\int\limits_{300nm}^{3000nm} E(\lambda).d\lambda} \int\limits_{300nm}^{3000nm} E(\lambda)\rho_h(\lambda)d\lambda, \qquad (2)$$

As instruments usually acquire data in a limited number of wave bands, we estimated canopy hemispherical reflectance

values in each wave band using a multiple linear regression process, with the hemispherical reflectances values in the selected wave bands considered as independent variables. This approach is similar to that of *Price* [1990]. The six wave bands are similar to those of several Earth observation satellites (445, 560, 665, 855, 1650, and 2200 nm). We developed the relationship over 48 of the 77 canopies (grassland, sparse vegetation, and bare soil) for which Myneni's program was running fast enough to minimize the already important computation time. For these 48 canopies, in addition to the hemispherical reflectance values already computed in the six selected wave bands, we computed the hemispherical reflectance in 40 contiguous 50 nm width wave bands covering the 400-2500 nm spectral domain. As input data for the leaf and soil optical properties models are available only in the 400-2500 nm range, the 300-3000 nm spectral domain was reduced to 400-2500 nm. The error associated with this approximation is small since there is very little energy reaching the canopy in the 300-400 nm and 2500-3000 nm as compared to the 400-2500 nm range. A linear
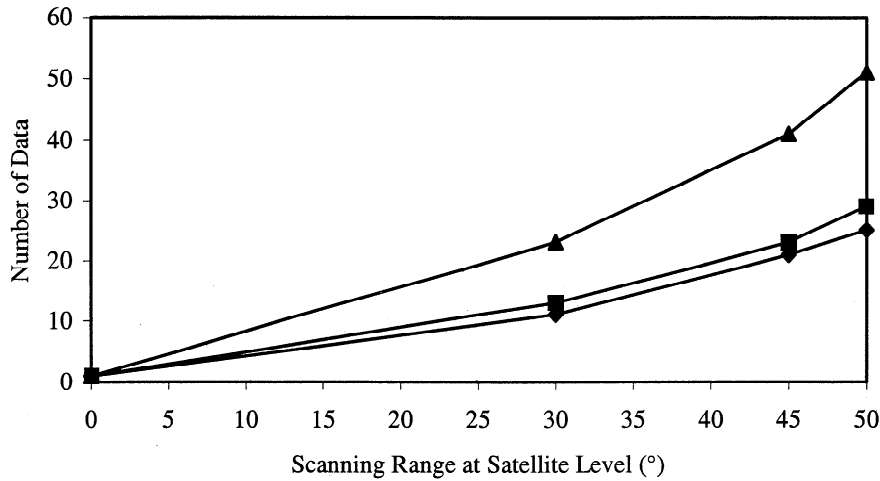
Figure 2. Number of data points acquired during the 32 day PRISM orbital cycle as a function of the scanning range at satellite level corresponding to the three across-track directional sampling capacities of the satellite ($\pm 30°$, $\pm 45°$, and $\pm 50°$). Computations were performed for the three latitudes of observation (diamonds, 0°; squares, 30°; triangles, 60°).

regression was then developed between the hemispherical reflectance of each of the 40 wave bands and the hemispherical reflectances corresponding to the n ($2 \le n \le 6$) selected wavelengths of the sensor:

$$\rho_h(\lambda_l) = \sum_{i=1}^{n} \alpha(\lambda_i, \lambda_l) \rho_h(\lambda_i), \qquad (3)$$

Thus combining (2) and (3) allows evaluation of the albedo from the hemispherical reflectances observed in the n wave bands:

$$a = \frac{1}{\int_{300nm}^{3000nm} E(\lambda)d\lambda} \int_{300nm}^{3000nm} E(\lambda)\rho_h(\lambda)d\lambda$$

$$a \approx \frac{1}{\int_{400nm}^{2500nm} E(\lambda)d\lambda} \int_{400nm}^{2500nm} E(\lambda)\rho_h(\lambda)d\lambda$$

$$a \approx \frac{1}{\sum_{l=1}^{40} E(\lambda_l)} \sum_{l=1}^{40} E(\lambda_l)\rho_h(\lambda_l) \qquad , \qquad (4)$$

$$a \approx \frac{1}{\sum_{l=1}^{40} E(\lambda_l)} \left[\sum_{l=1}^{40} E(\lambda_l) \left(\sum_{i=1}^{n} \alpha(\lambda_i, \lambda_l)\rho_h(\lambda_i) \right) \right]$$

$$a \approx \frac{1}{\sum_{l=1}^{40} E(\lambda_l)} \sum_{i=1}^{n} \rho_h(\lambda_i) \sum_{l=1}^{40} \alpha(\lambda_i, \lambda_l) E(\lambda_l)$$

The incoming solar radiation at the top of canopy level was computed using the 5S model with typical atmosphere characteristics. For each of the 40 wave bands, the performance of the regression is evaluated using root mean square error (RMSE) and relative RMSE (RRMSE):

$$\text{RMSE} = \sqrt{\frac{1}{k} \sum_{i=1}^{k} (x - \hat{x})^2} \quad \text{RRMSE} = \frac{\text{RMSE}}{\bar{x}}, \qquad (5)$$

where k is the size of the sample, x is the actual value, $\bar{x}$ is the average actual value, and $\hat{x}$ is the estimated value.

When the linear regression is based on the six selected wave bands (PRISM or MODIS instruments), the results show that the hemispherical reflectance is accurately estimated in any 50 nm wave band with a RMSE lower than 0.015 (Figure 3). The estimation is slightly poorer in the near infrared region (higher values of RMSE) mostly because of the lack of selected wave bands between 900 and 1300 nm. This effect could be minimized by using the MODIS wave band centered at 1240 nm or additional bands present on the PRISM instrument. An increase of the RMSE is also observed when the number of wave bands used for the regression is decreased (Figure 3). In the visible range, estimation was poorer when using only NOAA red and infrared bands (RMSE = 0.024). The estimation improved up to that of MERIS and PRISM (RMSE=0.007). Since NOAA, MSG, MERIS, and MISR have no wave band in the middle infrared region around 1650 nm, higher *RMSE* values were found than for VEGETATION in the near infrared and middle infrared

Table 2. Cloud Cover Derived From ISCCP Database.

	Tropical Forest	Grassland	Grassland/ Boreal Forest	Sparse Vegetation
Latitude/Longitude	4° / 55° W	37° / 95° W	65° / 100° E	13° / 5° E
DOY 80	-	-	32	46
DOY 172	45	50	68	56
DOY 355	-	-	-	19

Cloud cover in percent. For each case, latitude and longitude were chosen to correspond most closely to the simulations. DOY, day of the year
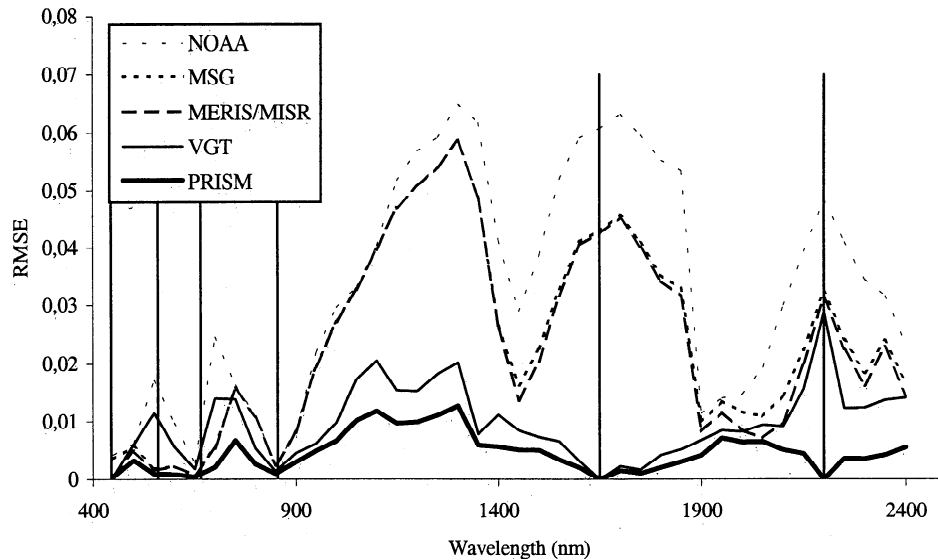
Figure 3. RMSE values associated with the estimation of hemispherical reflectance at a particular wavelength using the linear regression (equation (3)) and various sets of wave bands as presented in table 3. The vertical solid lines correspond to the six wavelengths alternatively used for the regression. The RMSE was computed over 48 canopy types.

regions. Estimates were better with more wavelengths and when they were placed more evenly along the spectrum.

Table 3 reports the contribution of each wave band to the albedo estimation. The visible bands always made the highest contribution. Also noted was a high contribution of the blue band for VEGETATION and PRISM or MODIS sensors. This could lead to significant errors, because the blue band usually has significant noise resulting from the atmospheric correction.

Because the algorithm does not consider the influence of the Sun position (since the regression is applied for the Sun angles determined by the latitude, the date, and the time of each simulation), complementary computations were performed to evaluate this possible influence. A large range of grassland types, with different soil background reflectance, was simulated for various Sun positions. We compared the fitting for the linear regression for each Sun zenith angle to that for all the Sun positions when using the six wave bands together. Results showed that albedo estimates for all positions were only slightly less accurate (RMSE=0.0042) than the estimates when considering each position explicitly (RMSE=0.0036). Thus the regression was almost completely insensitive to the Sun position.

3.2. Hemispherical Reflectance and Albedo Estimates From Top of Canopy Bidirectional Reflectance

To this point we have assumed that the hemispherical reflectance in the six selected wave bands was known. This is not the case, however, since most instruments do not sample fully the entire hemisphere. Thus this section describes using a BRDF model to derive hemispherical reflectance from bidirectional reflectance data observed in only a few directions by the satellite sensors. Top of canopy reflectance data from the six wave bands previously selected were used, assuming no contamination by atmospheric effects.

3.2.1. Choice of the BRDF model. The choice of the BRDF model was based on several criteria.

1. The model should have no more than three to four parameters to be tuned. This is consistent with the relatively simple BRDF patterns and with the restricted number of directional observations generally available.

2. The model should be linear. This eases the adjustment process that resumes to a pseudo matrix inversion and makes the result independent on the spatial scale. However, nonlinear models that could be linearized for inversion are acceptable.

Table 3. Coefficients of Each Wave Band Used in Equation (4) for Albedo Estimation From the Top of Canopy Hemispherical Reflectances Observed for a Few Wave Bands.

	Blue (445 nm)	Green (560 nm)	Red (665 nm)	NIR (855 nm)	MIR$_1$ (1650 nm)	MIR$_2$ (2200 nm)	RMSE	RRMSE, %
NOAA			0.570	0.46			0.0104	3.1
MSG		0.68	0.080	0.35			0.0093	2.8
MISR/MERIS	0.06	0.69	0.001	0.35			0.0088	2.7
VEGETATION	0.25		0.130	0.32	0.24		0.0047	1.4
MODIS/PRISM	0.57	0.11	-0.310	0.32	0.13	0.04	0.0042	1.3

The set of wave bands used were those available on several earth observation instruments. The RMSE and relative RMSE (RRMSE) values were associated with the estimation of the albedo from the hemispherical reflectance data observed in the few corresponding wave bands are also presented. The coefficients used in Equation (4) are $\Sigma_l \alpha(\lambda_i, \lambda_l) E(\lambda_l)$.
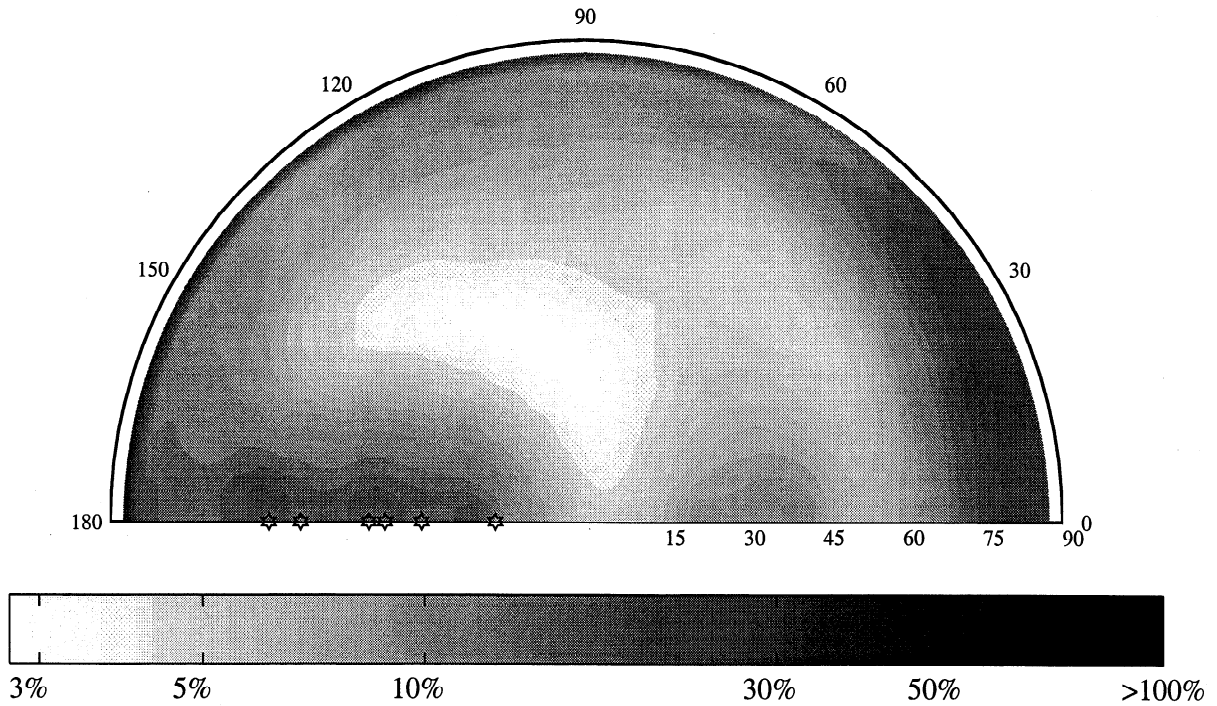
Figure 4. Polar representation of the RRMSE between actual and estimated BRDF values by inversion of the MRPV model over the whole BRDF. This error was computed over the 77 canopies for the six wave bands. The stars correspond to the Sun position for the different latitudes and dates of simulations.

3. The model does not need to be based on physics but should be flexible enough to accurately describe most situations.

4. The model should be reciprocal, that is, $\rho(\theta_s, \theta_v, \varphi) = \rho(\theta_v, \theta_s, \varphi)$. This will allow description of the variation of the BRDF with Sun position: hemispherical reflectance is often used for normalization processes that allow comparison of data acquired with the same sensor from one latitude (or date) to another and are therefore acquired at different solar angles. Moreover, general circulation models often require albedo
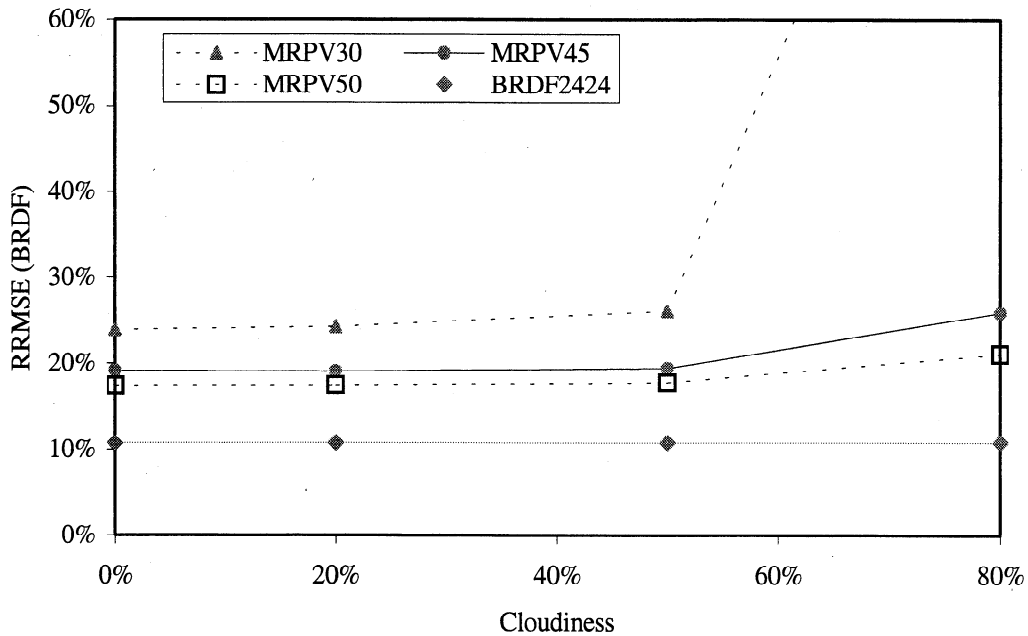

Figure 5. RRMSE values associated with the estimation of the BRDF in the 24 x 24 directions from reflectance data as sampled by the generic satellites for the three ranges of across-track viewing (±30°, ±45°, or ±50°), using the MRPV model. Results are provided for the 77 canopies for the six wave bands, as a function of cloud cover (0%, 20%, 50%, and 80%). The diamonds line corresponds to the RRMSE value when the model was inverted over the whole BRDF (24 x 24 directions).
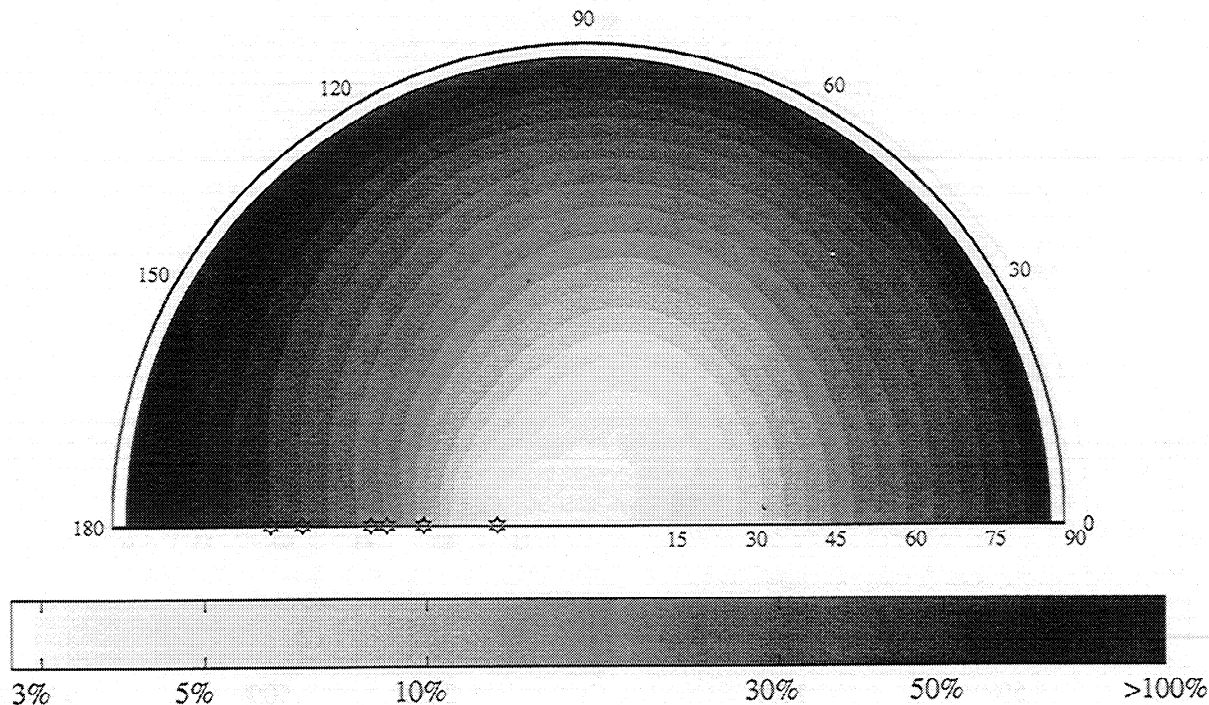
Figure 6. Polar representation of the RRMSE between actual and estimated BRDF values by inversion of the MRPV model over reflectance data as sampled by the generic satellites for the ±30° across-track viewing, considering 80% of clouds. This error was computed over the 77 canopies for the six wave bands. The stars correspond to the Sun position for the different latitudes and dates of simulations.

values integrated over the whole day, instead of instantaneous estimates.

Since hemispherical reflectance will be derived from a selection of viewing angles, the model must be able to extrapolate the BRDF throughout the hemisphere when inverted in a selection of viewing directions, for a given solar position. *Baret et al.* [1997] demonstrated that the Modified Rahman Pinty Verstraete (MRPV) [*Engelsen et al.,* 1996] and
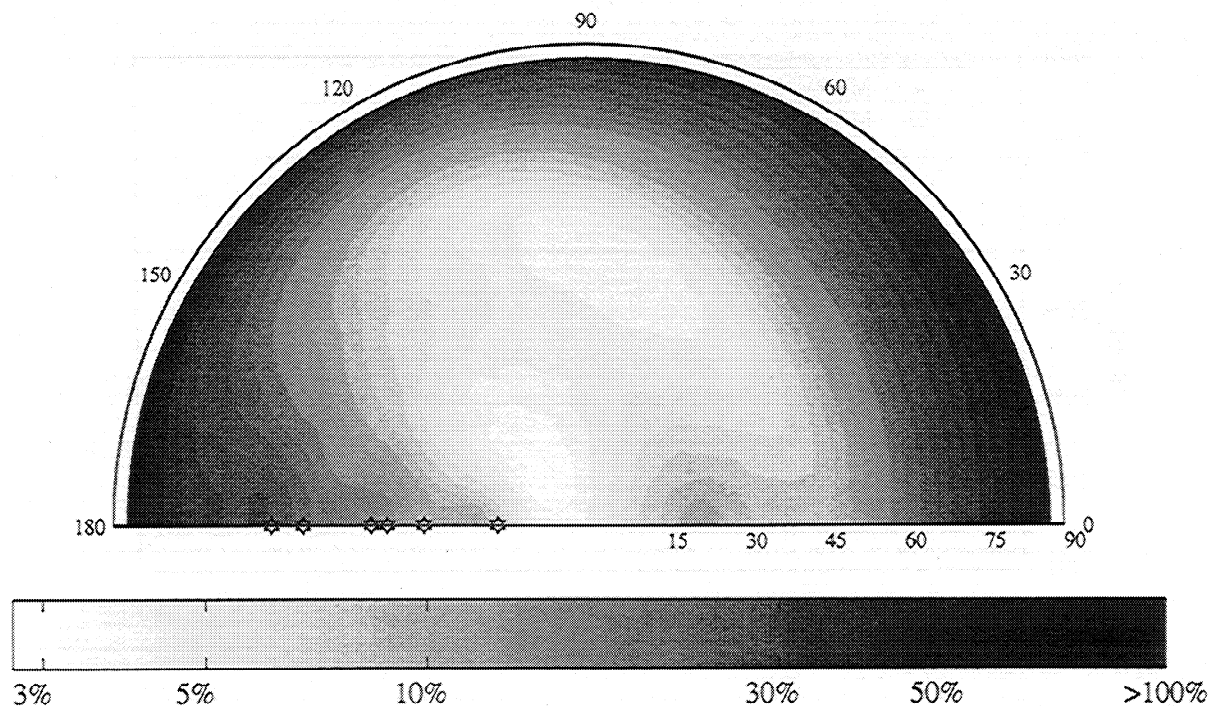

Figure 7. Polar representation of the RRMSE between actual and estimated BRDF values by inversion of the MRPV model over reflectance data as sampled by the generic satellites for the ±50° across-track viewing, considering 80% of clouds. This error was computed over the 77 canopies for the six wave bands. The stars correspond to the Sun position for the different latitudes and dates of simulations.

the modified Walthall's [*Walthall et al.*,1985; *Nilson and Kuusk*, 1989] models performed the best over most situations, as compared to Shibayama's [*Shibayama and Wiegand*, 1985] and Roujean's [*Roujean et al.*,1992] models. *Wanner et al.* [1997] also used the modified Walthall's model as a secondary product for the MODIS BRDF/albedo product, since it is very flexible in terms of describing the BRDF and can be used as a "universal model". This may produce higher RMSE values in many cases, however, when compared to models adapted to particular canopy types. The choice between MRPV and Walthall's models is driven by the results obtained by *Privette et al.* [1997] on measured data sets, and *Lucht* [1998] on a simulated database. They both compared the performances of the AMBRALS (Algorithm for MODIS bidirectional reflectance anisotropies of the land surface), MRPV, and Walthall's models [*Wanner et al.*, 1997] to estimate hemispherical reflectance from a given solar zenith angle at other solar positions. Results showed that both MRPV and AMBRALS models performed satisfactorily. We

therefore chose the MRPV model (three parameters) derived from *Rahman et al.* [1993]. It can be written in a semilinearized version:

$$\ln\frac{\rho(\theta_v,\theta_s,\phi)}{H} = \beta_1 + \beta_2 \ln[\cos\theta_s \cos\theta_v(\cos\theta_s + \cos\theta_v)] + \beta_3 \cos\xi$$

$$H = 1 + \frac{1-\overline{\rho}}{1+\sqrt{\tan^2\theta_s + \tan^2\theta_v - 2\tan\theta_s \tan\theta_v \cos\varphi}} \quad , (6)$$

H is the hot spot function, $\overline{\rho}$ is the average measured reflectance, and ξ is the phase angle. The hemispherical reflectance is computed by numerical integration of the MRPV model over the 24 x 24 quadrature directions.

3.2.2. Evaluation of MRPV model interpolation performances when fitting over the whole hemisphere.
First, the flexibility of the model was evaluated, that is its capacity to accurately fit the whole BRDF when inverted over
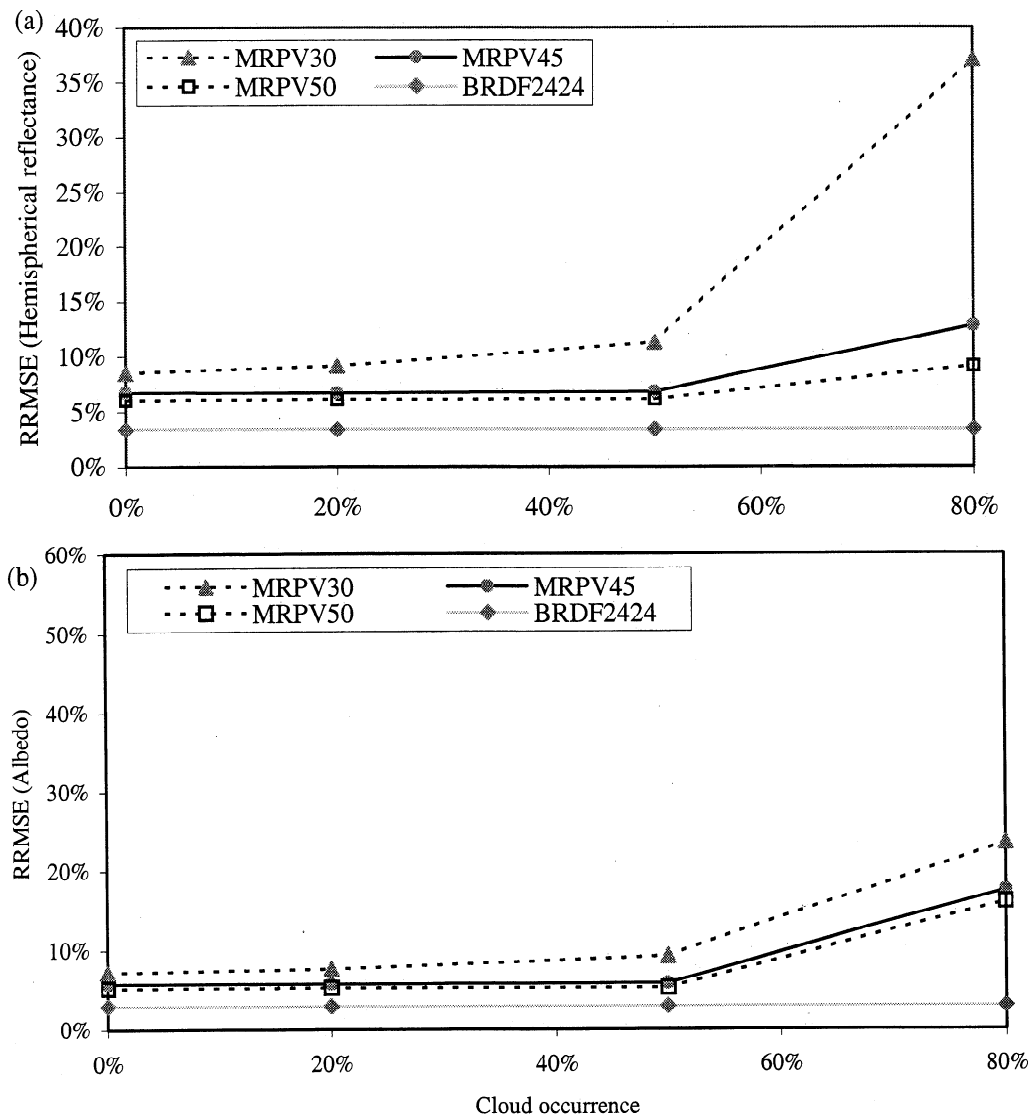

Figure 8. RRMSE values associated with the estimation of the (a) hemispherical reflectance and (b) albedo from the top of canopy bidirectional reflectance data as sampled by the generic satellites, for the three range of across-track viewing (±30°, ±45°, or ±50°), using the MRPV model. Results are provided for the 77 canopies for the six wave bands, as a function of cloud cover (0%, 20%, 50%, and 80%). The diamonds line correspond to the RRMSE value when the model was inverted over the whole BRDF (24 x 24 directions).

the whole BRDF. For each of the 77 canopies simulated, and each of the six wave bands, the model was inverted on the top of canopy BRDF in the 24 x 24 directions. The resulting coefficients of the model were then used to compute the BRDF in the Gaussian quadrature.

Results showed a good match between the BRDF computed with Myneni's radiative transfer model and the one derived from the model inversion. The RRMSE was 11% for MRPV when computed for all the six wave bands, the 77 canopies, and the 24x24 directions. The distribution of the RMSE between the estimated BRDF and Myneni's one as a function of the view angles showed good performances of the model except for large zenith angles and hot spot direction, demonstrating that the MRPV hot spot function is not well designed (Figure 4).

3.2.3. Evaluation of the MRPV model extrapolation performances when fitted over a selection of view directions. After demonstrating good interpolation capacities of the MRPV model, it was necessary to evaluate the extrapolation capacities for estimating the hemispherical

reflectance and the albedo, when only part of the BRDF was sampled by the satellite. Three scenarios were chosen for across-track view angles (±30°, ±45°, and ±50° at satellite level) and five cloud cover values (0%, 20%, 50%, 80% and ISCCP). To get a proper comparison of the three directional sampling capacities tested, all the data selected for ±30° were also selected for ±45° and all the data selected for ±45° were also selected for ±50°.

The goodness of the fit between Myneni's BRDF and that obtained using the model inverted over the sampled BRDF was slightly lower than that obtained when the model is inverted over the 24 x 24 Gauss quadrature directions (Figure 5). This demonstrated the generally good extrapolation performance of the MRPV model. However, for 80% cloud cover, there was a sharp increase in RRMSE values, particularly for the restricted directional sampling range (±30°). Figures 6 and 7 show the distribution of the RRMSE between the estimated BRDF and Myneni's one as a function of the view angles, when considering a ±30° or ±50° directional sampling, for 80% cloud cover. The MRPV model
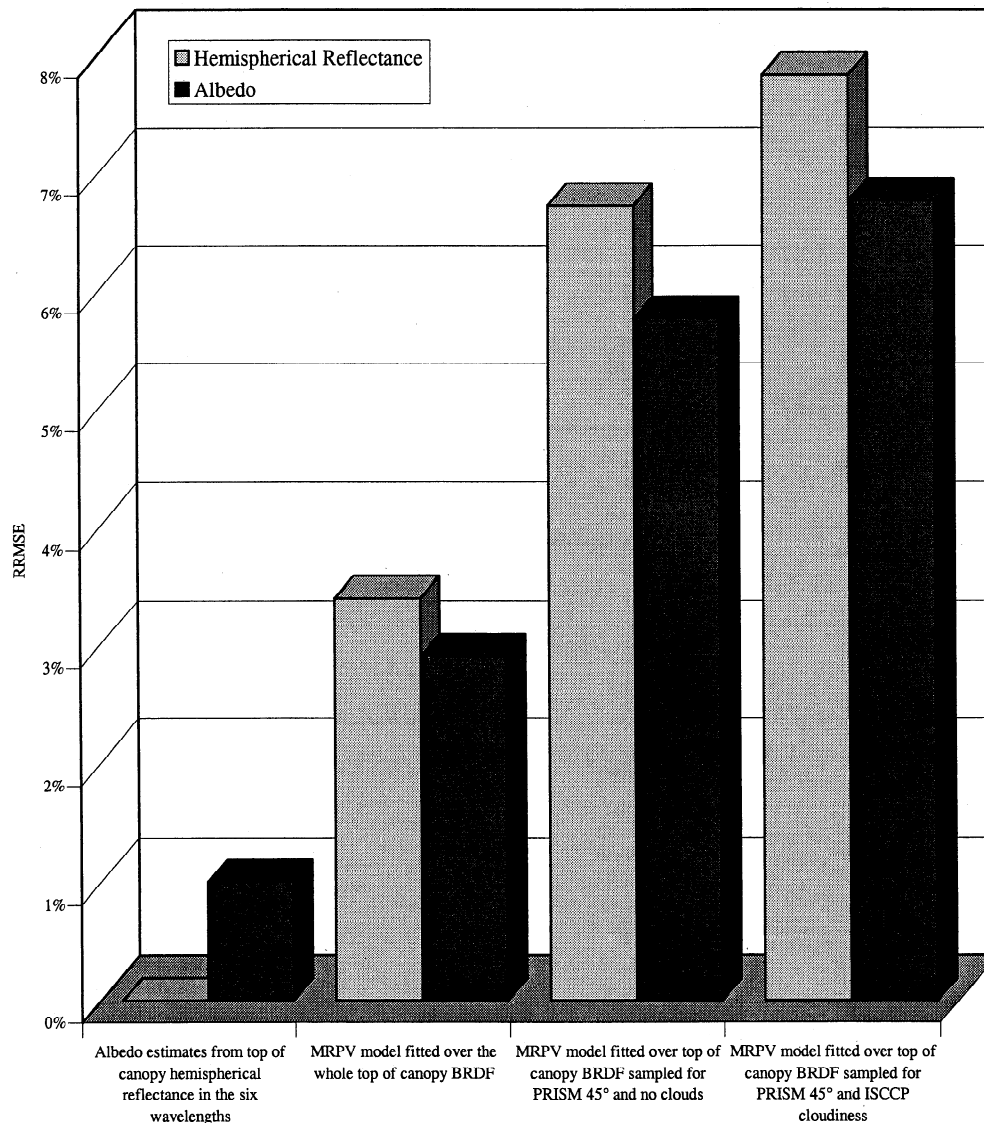

Figure 9. Error budget (RRMSE) of the estimation of the top of canopy hemispherical and albedo values at various stages of the process. The 77 canopies, the six wave bands, the ±45° across-track directional sampling scenario, and the ISCCP cloud percentage were considered.

provided good interpolation performances for zenith angles less than 30° (or 50°). Conversely, the RRMSE value increased drastically when extrapolating to larger zenith angles. For the ±50° scanning range we observed higher RRMSE values in the hot spot direction.

The goodness of the fit thus depend not only on the range of viewing angles but also on the number of data available to invert the BRDF model. For low latitudes this can be critical since there might be almost the same number of view directions as the number of parameters to be adjusted. This would lead to inconsistent estimates of the parameter values and thus to large errors in the simulated BRDF.

3.2.4. Hemispherical reflectance and albedo estimates. MRPV model provided good estimates of the hemispherical reflectance (RRMSE = 3.4%) when fitted over the whole BRDF. The fitting between estimated and actual albedo values, computed using the six wave bands was also very good, with a RRMSE of 2.9%. Estimates of hemispherical reflectance and albedo derived from the MRPV model adjusted to the selected view directions are significantly poorer than when adjusted over the 24 x 24 directions. This confirms that the integration of the BRDF, over the hemisphere, and then over the spectrum reduced the error between actual and estimated values by smoothing local errors of the model fitting.

For cloud cover values higher than 50%, increasing the range of view directions significantly improved the accuracy of hemispherical reflectance estimation (Figure 8a). In the case of the ±30° directional sampling scenario, the RRMSE was increasing with the cloud occurrence because the number of directions available became too few. Conversely, the higher ranges of directional sampling capabilities (±45° or ±50°) always provided enough data to allow a correct fit of the BRDF model. All the results presented for the hemispherical reflectance were very similar for albedo (Figure 8b), with slightly better performance due to the spectral integration that smoothes part of the inaccuracies of the model.

These results allowed presenting a budget error for the hemispherical reflectance estimation, showing that the main source of inaccuracy comes from the directional sampling scheme provided by the satellite and the capacity of the MRPV model to extrapolate the BRDF outside the range of observations (Figure 9). When considering the albedo estimation, spectral integration does not appear to be a major problem. Here again the main source of error lies in the directional sampling capacity of the satellite and the extrapolation performances of the BRDF model. Observations at the lower latitudes, where cloud cover could be quite high, would result in poorer estimates of hemispherical reflectance and albedo.

4. Conclusion

This study was based on a simulated data set of BRDF and hemispherical reflectance of a wide variety of land cover types representing the predominate biomes of the Earth's vegetated surface. Well-known and validated radiative transfer models were used for leaves, canopy, and soil background. The estimation of the hemispherical reflectance and albedo from generic Earth observation satellite data (such as those provided by NOAA, VEGETATION, MSG, MERIS,

MISR, MODIS, and PRISM) was divided in two steps using a bottom up approach.

1. The first step addressed the spectral integration issue at the top of canopy level. With few wave bands well distributed along the spectrum, it was possible to estimate the albedo with a relative accuracy of approximately 1%. This suggests that the minimum optimal set of wave bands should be a red and a near-infrared band. Great improvements were observed when a middle infrared wave band was used. This was not actually investigated in the recent studies dedicated to albedo estimation where only the spectral albedo was considered [*Privette et al.*, 1997; *Lucht*, 1998].

2. The second step addressed the directional integration issue. This appears to be the main source of error introduced in the estimation of the hemispherical reflectance and albedo. This is partly due to the limited range of directions sampled combined with the limited capacity of the BRDF model to extrapolate outside the range of directions sampled. The high view zenith angles appear to be quite critical because of their important contribution to the hemispherical reflectance. Thus research is needed for improving both the BRDF model and the way it is inverted/fitted over the observed view directions. Results are very consistent with those found by *Privette et al.* [1997] and *Lucht* [1998].

In the budget error presented we did not consider the atmospheric effects, instrumental errors, or the inaccuracies induced by the nonperfect coregistration of pixels between the several bands, and between the several directions and dates of observation. These factors can be quite important, particularly when using high spatial resolution data.

The derivation of hemispherical reflectance and albedo is based on the accumulation of observations along the 32 days orbit cycle, implicitly assuming no significant changes of the vegetation during this period. In many cases the vegetation will vary significantly within this 32 day period. It should thus be very interesting to investigate the degradation of the estimation when the accumulation period is shortened. Sensors such as POLDER or MISR are of great interest for this kind of application since they provide multiangle data acquired at the same time. Efforts should also focus on the combined use of data coming from several satellites, providing improved temporal, directional, and spectral sampling capacities.

References

Baret, F., M. Weiss, M. Leroy, O. Hautecoeur, R. Santer, and A. Bégué, Impact of surface anisotropies on the observation of optical imaging sensors, final report, *ESA contract 11341/95/NL/CN*, ESA, ESTEC, Netherland, 1997.

Del Bello, U., P. Kealy, R. Meynart, and M. Rast, PRISM: a hyperspectral imager for a future ESA land observation mission, paper presented at *European Satellite Remote Sensing Conference, ESA, Paris, France*, 25-28 september, 1995.

Deschamps, P.-Y., F. Bréon, M. Leroy, M. Podaire, A. Bricaud, J. Buriez, and G. Sèze, The POLDER mission: Instrument characteristics and scientific objectives, *IEEE Trans. Geosci. Remote Sens., 32*, 598-615, 1994.

Dickinson, R.E., Land surface processes and climate-surface albedos and energy balance, *Adv. Geophys.*, *25*, 305-353, 1983.

Diner, D.J, et al., Multi-angle Imaging SpectroRadiometer (MISR): Instrument description and overview, *IEEE Trans. Geosci. Remote Sens.*, *36*, 1072-1085, 1998.

Engelsen, O., B. Pinty, M. Verstraete, and J.V. Martonchik, Parametric bidirectional reflectance factor models: evaluation, improvements and applications, report EUR16426EN, *Eur. Comm., Joint Res. Cent., Space App. Inst.*, ISPRA, Italy, 1996.

Goutorbe J., et al., HAPEX-Sahel: A large scale study of land-atmosphere interactions in the semi-arid tropics, *Ann. Geophys.*, *12*, 53-64, 1994.

Hapke, B., Bidirectional reflectance spectroscopy, 1, Theory, *J. Geophys. Res.*, *86*, 3039-3054, 1981.

Hapke, B., Bidirectional reflectance spectroscopy, 3, Correction for macroscopic roughness, *Icarus*, *59*, 41-59, 1984.

Hapke, B., Bidirectional reflectance spectroscopy, 4, The extinction coefficient and the opposition effect, *Icarus*, *67*, 264-280, 1986.

Henderson-Sellers, A., and M.F. Wilson, Surface albedo data for climatic modeling, *Rev. Geophys*, *23*, 1743-1778, 1983.

Jacquemoud, S., and F. Baret, PROSPECT: A model leaf optical properties spectra, *Remote Sens. Environ.*, *27*, 157-167, 1990.

Jacquemoud S., F. Baret, and J.F. Hanocq, Modeling spectral and bidirectional soil reflectance, *Remote Sens. Environ..*, *41*, 123-132, 1992.

Kimes, D.S., and P.J. Sellers, Inferring hemispherical reflectance of the Earth's surface for global energy budgets from remotely sensed nadir or directional radiances values, *Remote Sens. Environ.*, *18*, 205-223, 1985.

Kimes, D.S., P.J. Sellers, and W.W. Newcomb, Hemispherical reflectance variations of vegetation canopies and implications for global and regional energy budget studies, *J. Clim. App. Meteorol.*, *26*, 959-972, 1987.

Lucht, W., Expected retrieval accuracies of bidirectional reflectance and albedo from EOS-MODIS and MISR angular sampling, *J. Geophys. Res.*, *103*, 8763-8778, 1998.

Myneni, R.B., A. Marshak, Y. Knyazikhin, and G. Asrar, Discrete ordinates method for photon transport in leaf canopies, in *Photon-Vegetation Interactions*, edited by R.B. Myneni and J. Ross, pp 46-109, Springer-Verlag, New York, 1991.

Myneni, R.B., G. Asrar, and F.G. Hall, A three-dimensional radiative transfer method for optical remote sensing of vegetated land surfaces, *Remote Sens. Environ.*, *41*, 105-121, 1992.

Nilson, T., and A. Kuusk, A reflectance model for the homogeneous plant canopy and its inversion, *Remote Sens. Environ.*, *27*, 157-167, 1989.

Olioso, A., H. Chauki, D. Courault, and J.P. Wigneron, Estimation of evapotranspiration and photosynthesis by assimilation of remote sensing data into SVAT models, *Remote Sens. Environ.*, *68*, 341-356, 1999.

Pinty, B., and D. Ramond, A simple bidirectional reflectance model for terrestrial surfaces, *J. Geophys. Res.*, *91*, 7803-7808, 1986.

Pinty, B., and M. Verstraete, On the design and validation of surface bidirectional reflectance and albedo model, *Remote Sens. Environ.*, *41*, 155-167, 1992.

Price, J.C., Information content of soil spectra, *Remote Sens. Environ.*, *33*, 113-121, 1990.

Privette, J.L., T.F. Eck, and D.W. Deering, Estimating spectral albedo and nadir reflectance through inversion of simple BRDF models with AVHRR/MODIS-like data, *J. Geophys. Res.*, *102*, 29,529-29,542, 1997.

Rahman, H., B. Pinty, and M.M. Verstraete, Coupled surface-atmosphere reflectance (CSAR) model, 2, Semi-empirical surface model usable with NOAA advanced very high resolution radiometer data, *J. Geophys. Res.*, *98*, 20,791-20,801, 1993.

Rossow, W.B., P.J. Gardner and A. Walker, International Satellite Cloud Climatology Project (ISCCP) documentation on cloud data, *Rep. WMO/TD 26*, 78 pp., World Meteorolo. Org., Geneva, Switzerland, 1988.

Roujean, J.L., M. Leroy, and P.Y. Deschamps, A bidirectional reflectance model of the Earth's surface for the correction of remote sensing data, *J. Geophys. Res.*, *97*, 20,455-20,468, 1992.

Sellers P.J., et al., BOREAS Experiment Plan (Version 3.0), *report*, NASA Goddard Space Flight Center, Greenbelt, Md., 1994.

Shibayama, M., and C.L. Wiegand, View azimuth and zenith and solar angle effects on wheat canopy reflectance, *Remote Sens. Environ.*, *18*, 91-103, 1985.

Shibayama, M., T. Akiyama, and K. Munakata, A portable field ultrasonic sensor for crop canopy characterization, *Remote Sens. Environ.*, *18*, 269-279, 1985.

Strahler, A.H., C.B. Schaaf, J.-P. Muller, W. Wanner, M.J. Barnsley, R. d'Entremont, B. Hu, P. Lewis, X. Li, and E.V. Ruiz de Lope, MODIS BRDF/albedo product: Algorithm theoretical basis document, *NASA EOS-MODIS Doc. Incl. Update*, version 4.0, 252pp., 1996.

Tanré, D., C. Deroo, P. Duhaut, M. Herman, and J.J Mocrette, Description of a computer code to simulate the satellite signal in the solar spectrum: The 5S code, *Int. J. Remote Sens.*, *11*, 659-668, 1990.

Verstraete, M.M, B. Pinty, and R.E. Dickinson, A physical model of the bidirectional reflectance of vegetation canopies, 1, Theory. *J. Geophys. Res.*, *95*, 11,767-11,775, 1990.

Walthall, C.L., J.M. Norman, J.M. Welles, G. Campbell, and G.L. Blad, Simple equation to approximate the bidirectional reflectance from vegetative canopies and bare soil surfaces, *App. Opt.*, *24*, 383-387, 1985.

Wanner, W., X. Li, and A.H. Strahler, On the derivation of kernels for kernel-driven models of bidirectional reflectance, *J. Geophys. Res.*, *100*, 21,077-21,090, 1995.

Wanner, W., A.H. Strahler, B. Hu, P. Lewis, J.-P. Muller, X. Li, C.L. Barker Schaaf, and M.J. Barnsley, Global retrieval of bidirectional reflectance and albedo over land from EOS MODIS and MISR data: Theory and algorithm, *J. Geophys. Res.*, *102*, 17,143-17,161, 1997.

F. Baret and M. Weiss, INRA Bioclimatologie, Site Agroparc, 84914 Avignon, Cedex 9, France. (weiss@avignon.inra.fr)

A. Bégué, CIRAD-CA, Maison de la Télédétection, 500, rue J.F. Breton, 34093 Montpellier, France.

O. Hautecoeur and M. Leroy, CESBIO, 18, avenue E. Belin, 31401 Toulouse Cedex, France.

R. Santer, LOA, Université du littoral, 62123 Wimereux, France.